Parameter optimization of electromagnetic pulse compaction driven by aluminum tube for tungsten copper powder

Fenqiang Li, Juehao Ding, Miao Zheng, Jianlin Xu, Xiaohong Ge, Hui Li and Jun Zhao

Fujian Provincial Key Laboratory of Functional Materials and Applications, School of Materials Science and Engineering, Xiamen University of Technology, Xiamen 361024, People's Republic of China

Abstract   A combination of multi-physics numerical simulation and experiment was conducted to study the magnetic pulse compaction technology driven by two aluminum tubes of tungsten copper powder. Then, the effects of different process parameters on the density and uniformity of the compact were studied by tuning the thickness of the pack and driver tubes and the gap between them. Results show that the density of compact is the highest when the thickness of the driver tube is 1.0 mm. More energy is consumed for force conduction as the thickness of the pack tube increases. Thus, the density of the compact is the highest when the thickness of the packer tube is 0.8 mm. The speed of the driver tube impacting the pack tube also increases with the rise in the gap. Accordingly, the compaction density with the gap of 1.5 mm is the highest under the same other parameters.

1. Introduction

W-Cu20 alloy has various excellent mechanical and electrical properties, such as high strength, high hardness, low thermal expansion, and good conductivity. It is widely used in metallurgical machinery, electronic information, national defense and military industry, aerospace, and other fields [1]. The main methods for preparing tungsten copper alloys at present include traditional methods (e.g., high-temperature liquid-phase sintering, infiltration, and activated liquid-phase sintering) and modern preparation methods (e.g., mechanical alloying, spark plasma sintering, coreduction, and 3D printing) [2, 3]. The infiltration method is the most widely used method to prepare high-tungsten W-Cu composites [4]. However, when the ordinary "powder mixing, molding, and sintering" process is used to prepare W-Cu alloy, the dissolution and precipitation mechanism in Kingery's theory [5] will not occur in the sintering densification process. This mechanism is mainly controlled by the particle rearrangement mechanism. As a result, the sintering density of composite materials is only 90 %-95 % of the theoretical density, and obtaining W-Cu alloy with high density is difficult.

Electromagnetic powder compaction (EMPC) is a new high-energy forming process that uses strong pulse electromagnetic force to act on the powder for densifying it. Its principle is to make the capacitor bank discharge through the inductor sheathed with or near the blank for generating pulse magnetic field with the help of the electromagnetic pulse compaction device. As a result, the induced current magnetic field in the blank interacts with the current magnetic field in the inductor. Then, the stored energy is transferred to the processed blank. The application of electromagnetic pulse forming technology in powder compaction at present has two compaction methods: electromagnetic powder radial compaction (EMPRC) using solenoid coil and electromagnetic powder axial compaction (EMPAC) using flat coil [6, 7]. The application of EMPRC to the compaction of W-Cu20 mixed powder is expected to solve the problem of low density by high-temperature liquid-phase sintering, which is a technical attempt worth studying.

In 1995, Chelluri et al. [8] put forward the dynamic magnetic compaction technology. In this technology, the powder is placed into a conductive container (clad shell) first. Then, it is placed

in the central cavity with high field strength. It is a kind of EMPRC. The whole compaction process takes a short time of less than 1 ms. This technology is suitable for manufacturing cylindrical symmetrical parts, thin-walled tubes, components with large height diameter ratio, and parts with complex internal shape. In 2014, Boltachev et al. [9] theoretically studied the magnetic pulse compaction of nano powder, analyzed the influence of inertia on the compaction process, and utilized the inertia characteristics of "mechanical powder and shell system." The dynamic magnetic pulse compaction method can achieve extremely high compaction pressure. Ref. [10] also mentioned that inertia effect can be effectively used in magnetic pulse compaction. The magnetic pressure can accelerate the shell walls to a high velocity when the powder density is sufficiently low. Then, the shell walls start to exert pressure and decelerate the magnetic and stored kinetic energies (and the latter can exceed the former by several folds).

The tooling configuration of solenoid coil EMPC also has two patterns. One is the single-tube compaction, which is widely used by many scholars at present. It was employed by Mamalis et al. [11] for near net-shape manufacturing of axisymmetric metal/superconducting YBCO ceramic compound billets, by Kabert [12] for Ti-6Al-4V tube compound billets, by Boltachev [13] for the forming of nanosized powders, and by Thirupathi [14] for the forming of Al 6061 alloy bar. The other way is the double-tube compaction, which is studied less. It was only used by Kabert [12] for Ti-6Al-4V tube compound billets. However, the parameter configuration should be studied further.

In this study, the magnetic pulse compaction technology of tungsten copper mixed powder driven by two aluminum tubes was studied by means of multi-physics field coupling numerical simulation and experiment. The influence of different process parameters on the density and density uniformity of the compact was investigated by changing the thickness of the pack and driver tubes and the gap between them.

2. Methods

2.1 Experiment

The materials used in the experiment are tungsten powder and copper powder produced by China Metallurgical Research Institute. The chemical composition of tungsten and copper powders are listed in Table 1. The morphological characteristics of these powders are shown in Fig. 1. The tungsten powder is of high purity and has a polygonal shape and a particle size of about 3 µm. The copper powder is also of high purity and has a wheat ear shape and a particle size of about 20 µm. The material of the pack and driver tubes is A1050 aluminum alloy. Static tensile test of A1050 aluminum alloy tube is accomplished using a universal testing machine. The results are illustrated in the stress vs. strain curve shown in Fig. 2.

The experimental device is shown in Fig. 3, and it includes an energy storage cabinet (including four sets of capacitors, C

Table 1. Chemical composition of materials.

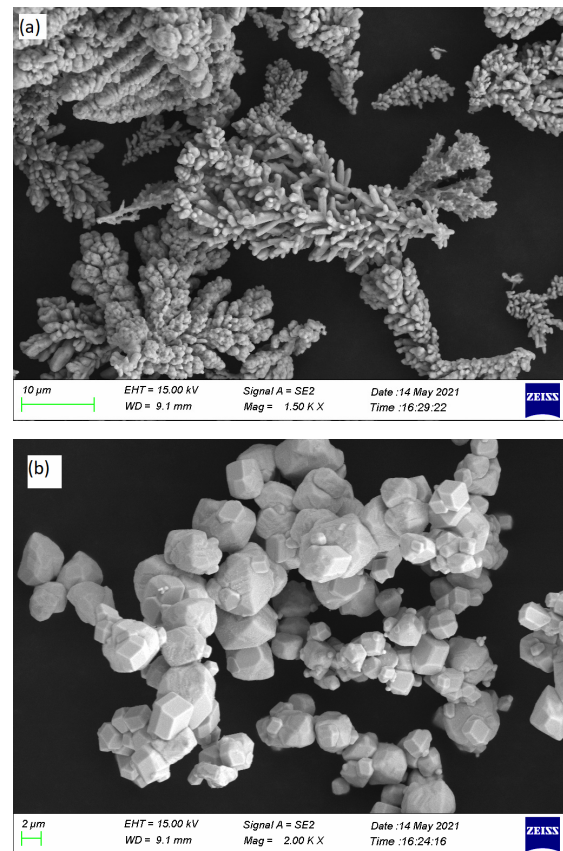| Original powder	Purity	Color
W	99 %	Dark gray
Cu	99 %	Purplish red

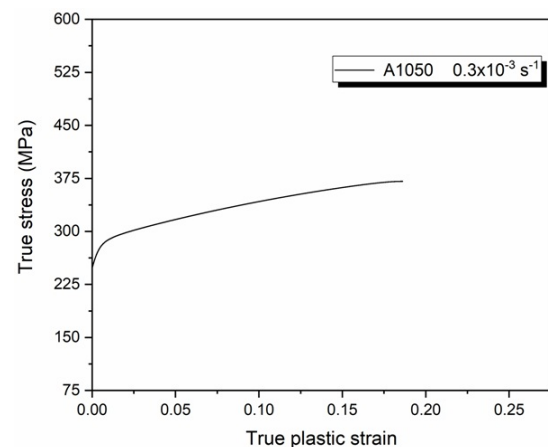Fig. 1. SEM diagram of the experimental powder: (a) copper; (b) tungsten.

Fig. 2. Quasi-static stress vs. strain curve of driver tube.

= 740 µf), a control cabinet, and a workbench. The workbench is equipped with radial compression coils and a field shaper. According to existing research results, low-frequency long
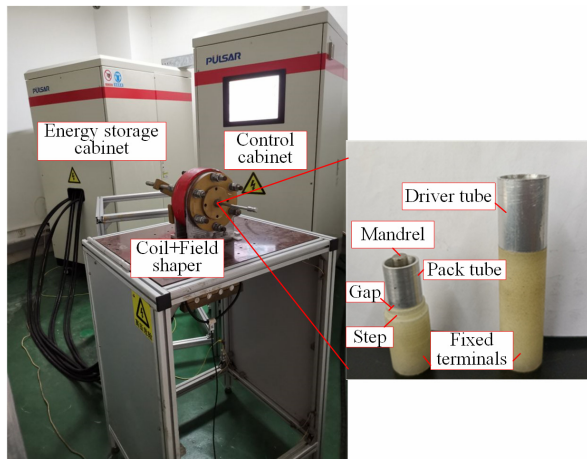
Fig. 3. Experimental equipment and tool.

Table 2. List of parameter combinations.

No.	Gap (mm)	t_{driver} (mm)	t_{pack} (mm)
Group 1	1.0	1.0	1.0
Group 2	0.5	1.0	1.0
Group 3	1.5	1.0	1.0
Group 4	1.0	1.0	0.8
Group 5	1.0	1.0	1.2
Group 6	1.0	1.2	1.0
Group 7	1.0	1.4	1.0
Group 8	1.2	1.0	1.0
Group 9	0.8	1.0	1.0
Group 10	1.0	0.8	1.0

pulses are beneficial to powder compaction. Thus, a multi-turn coil was used in this experiment. The nylon fixed terminal, stainless-steel mandrel, aluminum alloy pack tube, and aluminum alloy driver tube were processed according to the dimension of the field shaper. Before compaction, the stainless-steel mandrel and aluminum alloy pack tube were first installed on the nylon fixed terminal. The prepared W-Cu20 mixed powder was filled between the pack tube and the mandrel while vibrating to increase the initial packing density. The driver tube and another fixed terminal were plugged tightly, and the weight was measured to calculate the initial packing density. The assembled tool was placed into the field shaper, and the position was adjusted to ensure that the powder was within the length of the inner diameter of the field shaper. A discharge voltage of 7 kV was used for compaction, and a Rogowski coil was utilized to measure the current flowing through the coil. After compaction, the imageJ software was used to measure the diameter of the driver tube at different locations for calculating the deformation displacement of the driver tube and the density distribution of W-Cu20 compact.

2.2 Numerical simulation

The numerical simulation method described in Ref. [15] was used for the magnetic pulse radial compaction in this study. The electromagnetic simulation model was set up using ANSYS/EMAG software, and the coil was modeled into a current-fed conductor with a zero voltage drop applied to one end of the coil. The total number of coil turns was 5. The current degree of freedom at the other end of the coil was coupled, and the current load was applied. The profile of discharge current was recorded by an oscilloscope using a Rogowski coil during the discharge process. The corresponding boundary conditions were applied to the model, and the distribution of electromagnetic force on the driver tube could be calculated.

A mechanical model was established in the ABAQUS /Explicit finite element software, in which the driver tube, pack tube, powder, mandrel, and fixed terminals were modeled us-

ing C3D8R solid elements. The deformation of the driver and pack tubes could be calculated according to the material constitutive equation under high strain rate, that is, the Cowper-Symonds constitutive model, while applying the electromagnetic node load and the corresponding boundary condition to the mechanical model. The mechanical properties and the true stress vs. true strain of the component materials under quasi-static state were all the same as those in Ref. [15]. A modified Drucker-Prager cap model was used in this study to write the VUSDFLD subroutine for reproducing the W-Cu20 powder compaction behavior. Then, the density and stress distribution in the powder compaction process were predicted. The relationship between the material parameters and relative density can be found in Ref. [15].

The discharge voltage was kept unchanged at 7 kV in investigating the effect of the thickness of driver and pack tubes and the gap between them on the density and density uniformity of the compact. The skin depth of the aluminum tube in the condition was calculated to be 1.2 mm. According to the existing tooling size, the density and density uniformity of W-Cu20 compact were analyzed using 10 groups of parameter combinations as listed in Table 2.

3. Results and discussion

3.1 Density of the compact over time

The analysis of several groups of numerical simulation results showed that the density of the compacts changed with time in a consistent manner. Therefore, group 1 was selected in this study for analysis. Fig. 4 shows the curve of density varying with time at the axial center of the outer layer of the compact. The initial density of loose powder was 50 %. The driver tube impacted the pack tube at about 13 μs, and then, the force was transferred to the powder. The outer center of the compact deformed, and the density increased rapidly. When the compaction was in a certain degree, the reaction force between the powders increased due to the gradually smaller gap between the powders, and the density increased slowly. As the compaction continued, the reaction force be-
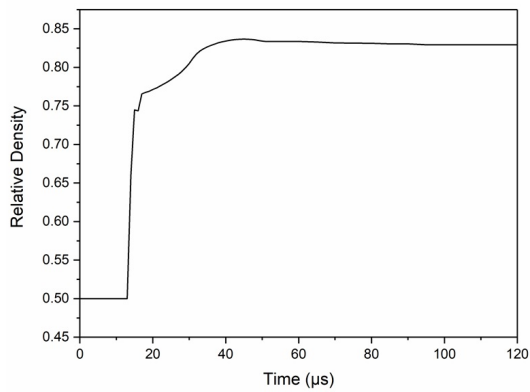
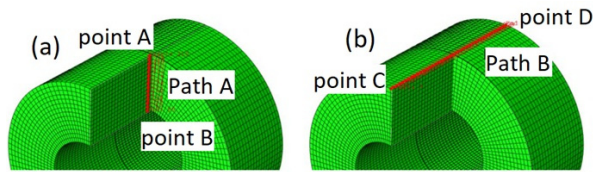Fig. 4. Density of center position of outer surface of compact changing with time.

Fig. 5. Definition of analysis paths: (a) path A with different thicknesses in the middle of the compact; (b) path B of the outer layer of the compact.
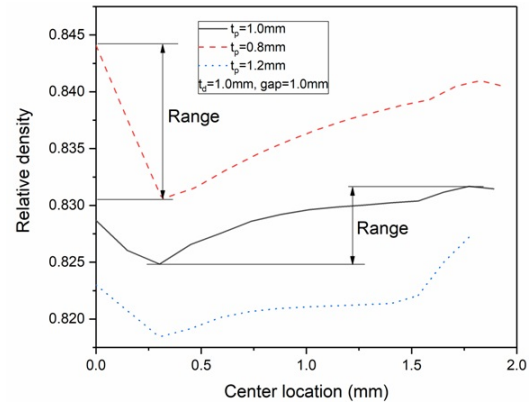

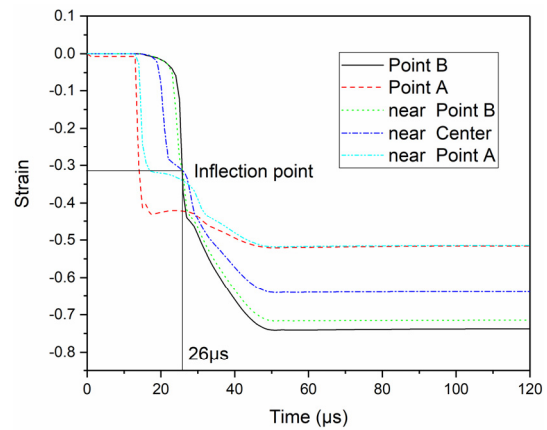Fig. 6. Density distribution along path A of compacts after compaction with different thicknesses of pack tubes.

Fig. 7. Strain vs. time curves for layers of different thicknesses along path A.

tween the powders increased gradually and the density reached the maximum value at 45 μs, and then, it began to decrease. Notably, the electromagnetic force was maximum at the first quarter cycle, which was about 45 μs. The density decreased slightly after 45 μs due to the reverse expansion of electromagnetic pulse compaction at half cycle and the spring-back of metal powder.

3.2 Spatial distribution of the density

As shown in Fig. 5, the path A selected from the upper (point A) to the lower (point B) was used to analyze the distribution of density of different thicknesses at the center of the compact, and the path B selected from the left (point C) to the right (point D) was used to analyze the density distribution of the outer layer of the compact. The following figures are all drawn based on the two paths.

3.2.1 Effect of the thickness of pack tube

Fig. 6 shows the density distribution of the compact along path A after compaction using pack tubes with different thicknesses. The figure indicates that the density near the mandrel and the surface layer was relatively high. When the thickness of the pack tube was thin, the highest density appeared in the outer layer of the compact. The highest density was transferred to the position close to the mandrel when the thickness of the pack tube was thickened. The pack tube was thinner, the driving energy was higher, and the density was higher. However, the density range was large and the density uniformity was poor, as shown in Fig. 6. The existence of the mandrel sharply

increased the deformation near the mandrel, and the time of transformation was about 26 μs, as shown in Fig. 7. Fig. 7 shows the change curve of strain over time at different locations along path A.

The cloud chart of powder density at different times is shown in Fig. 8. At 25-27 μs, the driver tube impacted the pack tube and compacted the powder. At 25 μs, the driver tube impacted the pack tube and pressed the powder. As a result, the density of the outer layer of the powder was high. When the transmission of force was conducted for 27 μs, an external force was observed on the surface layer and the layer near the mandrel simultaneously. The densities of the outer layer and near the mandrel were high, while the density in the middle was low. This result is due to that the force of the driver tube and the reflected force transmitted to the mandrel collided, which resulted in a decrease in density. Therefore, the density distribution would also show a waist shape.

The density distribution along the path A of the compact with the pack tube thickness of 1.0 mm at 60 and 120 μs is shown in Fig. 9. The powder density at the mandrel when the compact was pressed for 60 μs was higher than that at 120 μs. This result is attributed to the reverse expansion response and the
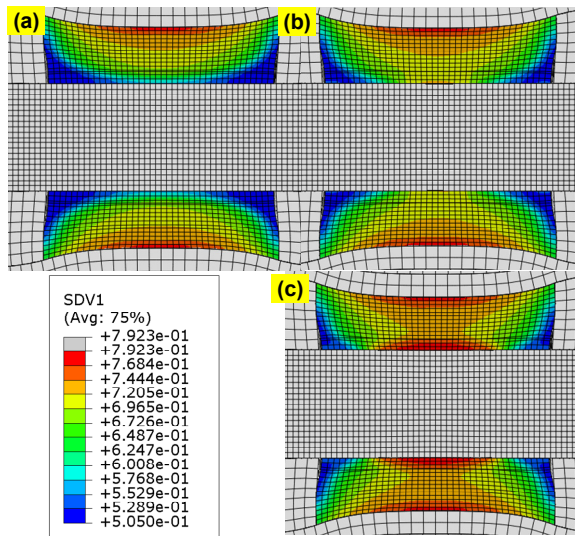
Fig. 8. Density distribution of compact at different times: (a) time when the pack tube contacts the powder (25 µs); (b) force being transmitted to the mandrel (26 µs); (c) mandrel rebounding (27 µs).
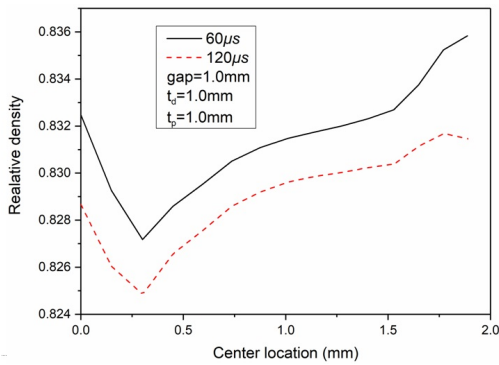

Fig. 9. Density distribution along path A of compact after compaction for 60 and 120 µs.
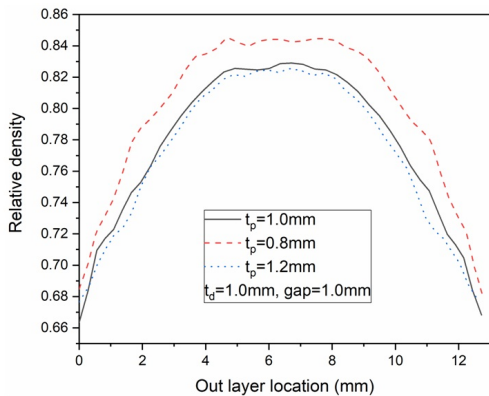

Fig. 10. Density distribution of outer surface layer of compact under different pack tube thicknesses.

springback of the metal powder.

Fig. 10 shows the density distribution of the outer layer of the compact along path B under the conditions of different pack
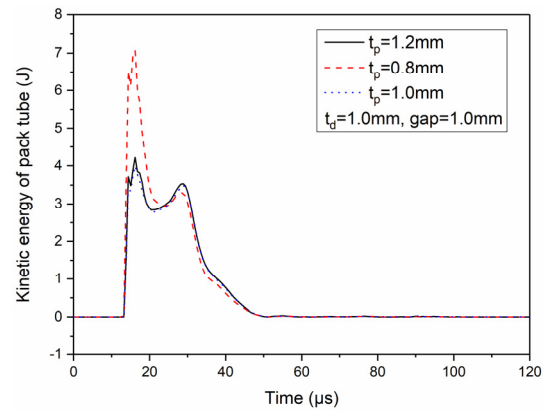

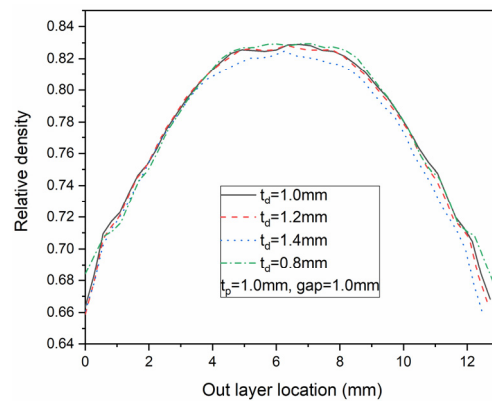Fig. 11. Kinetic energy of pack tubes with different thicknesses changing with time.

Fig. 12. Density distribution along path B using different driver tube thicknesses.

tube thicknesses. The density within 2 mm on the left and right of the path center was relatively high. During compaction, the force transmission on both sides of the driver tube would be greatly weakened due to the obstruction of the steps. As a result, the density could reach a higher level only at the center. Obviously, the compaction effect of the pack tube thickness of 0.8 mm was better than that of 1.0 and 1.2 mm. The obtained kinetic energy was greater when the pack tube was thinner, as shown in Fig. 11. The force on the powder was also greater. Thus, the final compact had higher density.

3.2.2 Effect of the thickness of driver tube

Fig. 12 shows the density distribution along path B after compaction in the condition of different driver tube thicknesses. Obviously, the difference in density was small. Fig. 13 shows the density distribution along path A after compaction with different driver tube thicknesses. The overall curve trend was the same as that of different pack tube thicknesses in Sec. 3.2.1. However, at the position of 0 mm (i.e., the outer layer), the densities were similar when the thicknesses of the driver tube were 0.8, 1.0, and 1.2 mm. Among them, the density with t_d = 1.0 mm was slightly higher, while the density with t_d = 0.8 mm coincided with that of 1.2 mm. Notably, t_d = 1.0 mm was the
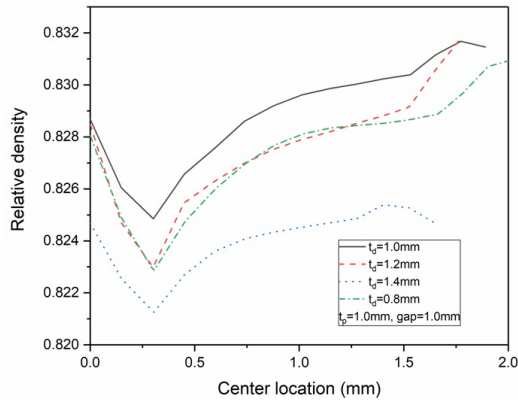
Fig. 13. Density distribution along path A using different driver tube thicknesses.
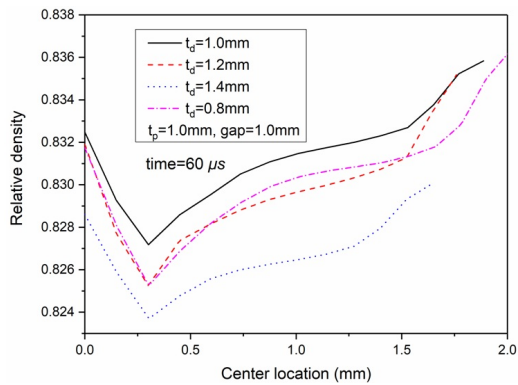

Fig. 14. Density distribution along path A using different driver tube thicknesses at 60 μs.

Fig. 15. Electromagnetic force on the driver tubes with different thicknesses.
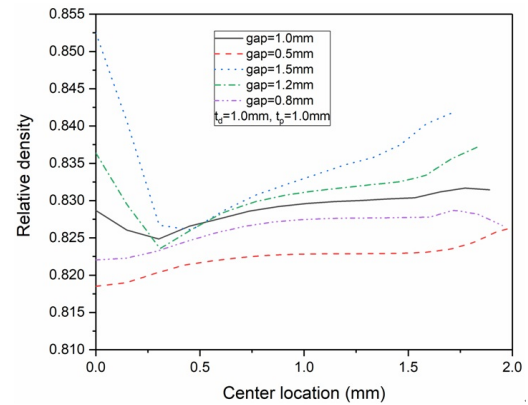
Fig. 16. Density along path A of compacts with different gaps.

closest to the skin depth and the driving force was the largest when the two other parameters were set to 1.0 mm. The driver tube with t_d = 0.8 mm suffered less electromagnetic force due to the skin effect. With regard to the driver tube with t_d = 1.2 mm, the plastic work consumed by self-deformation became larger. The density near the mandrel decreased when the thicknesses of the driver tube were 1.0 and 1.4 mm. The density distribution under different driver tube thicknesses at 60 μs is shown in Fig. 14. The density reduction is also caused by the reason mention before. The overall density distribution implied that the compacts had the highest density when the driver tube thickness was 1.0 mm, the densities were close when the driver tube thicknesses were 0.8 and 1.2 mm, and the powder density was the worst when the driver tube thickness was 1.4 mm.

The applied load was the first half wave of the sinusoidal attenuation current, and the current reached the maximum at 38.3 μs. Thus, the electromagnetic force distribution at 38.3 μs was extracted from ANSYS for analysis. The electromagnetic force on aluminum tubes with different driver tube thicknesses is shown in Fig. 15. The skin depth of aluminum alloy tube under this discharge parameter was slightly greater than 1.2 mm. The figure shows that the electromagnetic force on aluminum tube with a thickness of 1.4 mm was the largest but
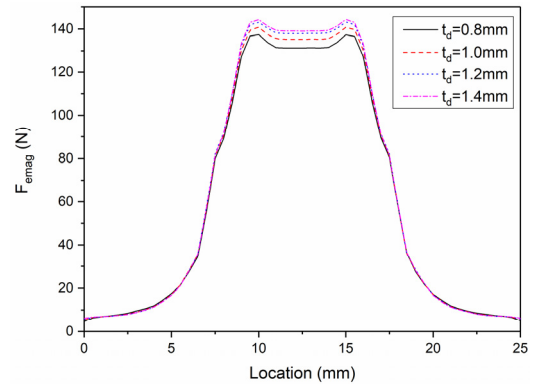
close to that with a thickness of 1.2 mm. The density of the compact using a driver tube with t_d = 1.0 mm was the highest, which is due to that the increase in electromagnetic force was insufficient to offset the extra energy consumed by the plastic deformation of the thickened driver tube. The density of the compact using a driver tube with t_d = 0.8 mm was low because the decrease in electromagnetic force suffered by the thin driver tube was insufficient to offset the reduction in the energy consumption for the plastic deformation of the thin tube.

3.2.3 Effect of the gap between the driver and pack tubes

Figs. 16 and 17 show the density distribution along paths A and B using different gaps between the driver and pack tubes. The curve trend was the same as that in Sec. 3.2.1. In the case of different gaps, the acceleration time of the driver tube was longer and the impact speed to the pack tube was greater when the gap was larger. The density of the central layer (Fig. 16) and the outer layer (Fig. 17) increased gradually with the rise in the gap. However, if the gap was too large, then the bending part of the driver tube would be too large, which would affect the contact area of the impact pack tube. Therefore, the gap should be controlled within a reasonable range according to the size of the field shaper.

Figs. 18 and 19 show the velocity distributions of the inner layer of the driver tube and the outer layer of the pack tube at the moment of contact between them in the condition of different gaps. A step was applied on the terminal to block the driver tube. Thus, the driver tube collided with the pack tube in a curved shape. The speed was exchanged during the collision, which resulted in that the speed of the inner layer of the driver tube showed a sharp drop at the center position. Moreover, the speed of the outer layer of the pack tube showed a high speed in the middle, and the speed of both sides was low. The collision speed was also great when the gap was larger, which increased the density. Therefore, the gap should be taken as a large value according to the size of the tool to obtain higher density.

3.3 Experimental verification

In this study, the reliability of the simulation model was verified by the experiment of parameter group 1, and the result of parameter optimization was verified by the experiment of group 4.

After compaction, the aluminum tube was difficult to collect from the nylon terminal due to its contraction. Thus, the imageJ software was used to measure the diameter of the center position for calculating the volume after compaction. The diameter at the center of the compact measured during the experiment of group 4 was 13.4 mm. According to the calculation method of compression density in Ref. [12], the quality before and after compression was assumed to be unchanged. Then,

$$
\begin{aligned}
\mathrm{m} = V_0 \rho_0 &= \rho_0 h \pi [(r_{p0} - t_p)^2 - r_{m0}{}^2] \\
&= V \rho = \rho h \pi \left[(r_d - t_d - t_p)^2 - r_{m0}{}^2 \right]
\end{aligned}
\tag{1}
$$

where r_{p0} is the initial outer diameter of the pack tube, r_{m0} is the initial outer diameter of the mandrel, r_d is the outer diameter of the driver tube after deformation, t_d is the thickness of driver tube, t_p is the thickness of pack tube, ρ_0 is initial relative density, h is powder height, and ρ is the relative density after compaction. From Eq. (1), we can obtain

$$
\rho = \rho_0 \frac{(r_{p0} - t_p)^2 - r_{m0}{}^2}{(r_d - t_p - t_d)^2 - r_{m0}{}^2} .
\tag{2}
$$

According to the volume and weight before and after the experiment, the relative densities measured before and after the optimization of the parameters were calculated by Eq. (2), as listed in Table 4.

The comparison between the experimental and simulation results is shown in Fig. 20. The curve is the data drawn from simulation, and the scatter points are the data calculated by Eq. (2). The max relative density of group 1 was 78.2 % as obtained from the experiment and was 82.9 % from the simulation, with a difference of only 4.7 %. Thus, the numerical model of
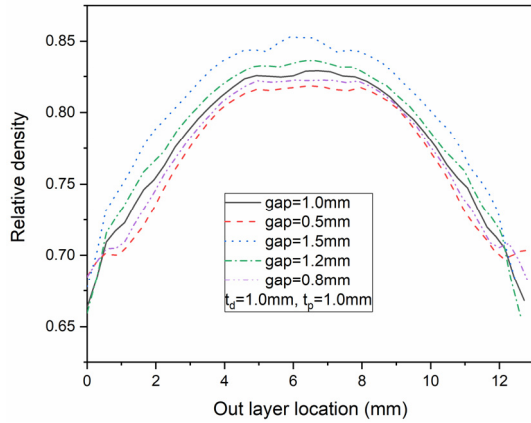

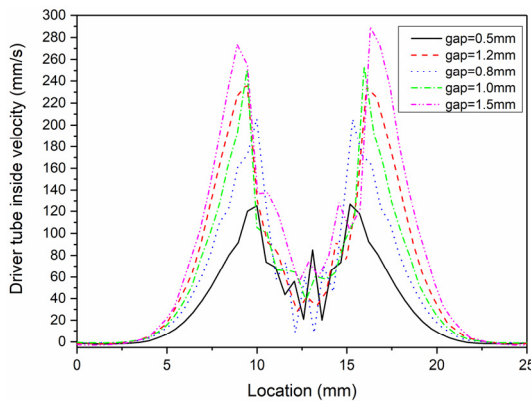Fig. 17. Density along path B of compacts with different gaps.

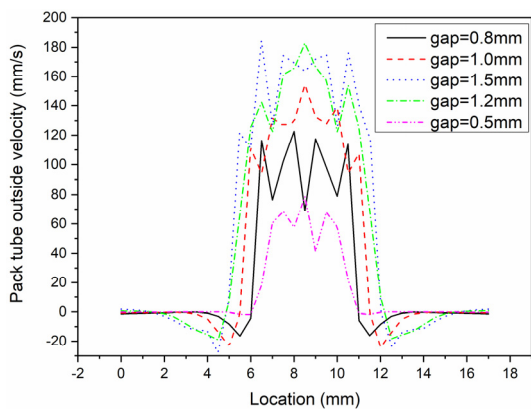Fig. 18. Velocity at the inner layer of driver tubes with different gaps.

Fig. 19. Velocity at the outer layer of pack tubes with different gaps.

Table 3. Relative density before and after compaction.

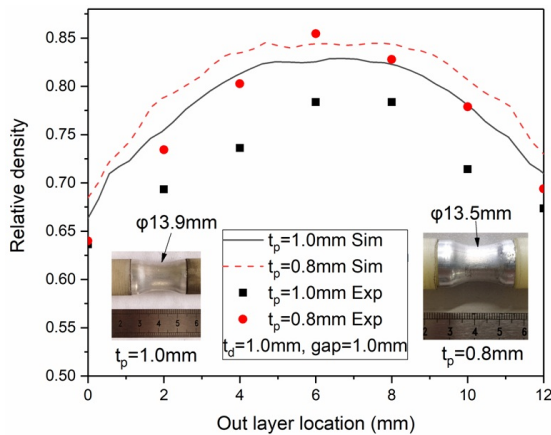| No.	Quality/g	Volume before/mm^3	Density before	Volume after/mm^3	Density after
1	5.97	848.23	45.0 %	488.11	78.2 %
4	6.50	924.88	45.0 %	471.31	85.5 %

Fig. 20. Comparison diagram of relative density along path B obtained by experiment and numerical simulation.

EMPC is reliable. After optimization analysis according to multiple groups of simulation results, the relative density in group 4 was 85.99 %. In the experiment, the relative density of 85.5 % after optimization was improved compared with 78.2 %. The result of parameter optimization is also reliable.

3.4 Further studies

The double-tube material used for compaction in this study was aluminum material, and copper material would be considered in the future. In the form of driver and pack tubes, multi-layer foil layer can be used by winding, which is convenient for collecting the compact after compaction. The evolution of force chains between particles is also worth studying.

4. Conclusions

The electromagnetic pulse radial compaction of W-Cu20 mixed powder with two aluminum tubes was simulated by commercial finite element software. The process parameters were optimized. The numerical model and optimization results were verified by experimental data. The main conclusions are as follows:

1) The thin pack tube can reduce the force conduction loss of the driver tube, and the density of the compact is higher when the pack tube is thinner. However, the density range is also larger, which means the density uniformity is poor. In addition, the density at the radial center of the compact is lower than those at the outermost layer and near the mandrel. The reason is that the stress wave of the driver tube collides with the stress wave rebounded from the mandrel.

2) The compaction effect is best when the driver tube thickness is 1.0 mm although the skin depth of the aluminum tube is 1.2 mm. The increase in electromagnetic force is insufficient to compensate for additional energy required for the deformation of the driver tube caused by the thickening.

3) The density of the compact is higher when the gap between the driver and pack tubes is larger. However, if the gap

is too large, then the bending part of the driver pipe will be too large. This condition will affect the contact area of the impact of pack tube. Therefore, the gap should be controlled within a reasonable range according to the size of the field shaper.

References

[1] J. Z. Hu, D. R. Li, B. Zhou, L. Q. Cui and Z. Y. Liu, Study on numerical simulation of W-Cu20 powder rolling based on Drucker-Prager/Cap model, *Powder Metallurgy Technology*, 35 (4) (2017) 249-253.

[2] W. Feng, Y. Li and X. Zhu, Preparation and application of W - Cu composites, *Journal of Chengdu University (Natural Science Edition)*, 30 (4) (2011) 364-367.

[3] Y. Wang, L. Zhuo and E. Yin, Progress, challenges and potentials/ trends of tungsten-copper (WCu) composites/pseudo-alloys: fabrication, regulation and application, *International Journal of Refractory Metals and Hard Materials*, 100 (2021) 105648.

[4] Y. Tao, Z. Wang, N. Fang and Z. Wu, Manufacture methods of tungsten-copper composites, *Powder Metallurgy Technology* (1) (2002) 49-51 (in Chinese).

[5] W. D. Kingery, Densification during sintering in the presence of a liquid phase, *Journal of Applied Physics*, 30 (3) (1959) 301-306.

[6] Z. Chen, *Modern Powder Metallurgy Technology*, Chemical Industry Press (2013) 327 (in Chinese).

[7] F. Q. Li, J. Zhao, J. H. Mo, J. J. Li and L. Huang, Comparative study of the microstructure of Ti-6Al-4V titanium alloy sheets under quasi-static and high-velocity bulging, *Journal of Mechanical Science and Technology*, 31 (3) (2017) 1349-1356.

[8] B. Chelluri and J. P. Barber, *Method for Compaction of Powder-Like Materials*, U.S. Patent 5405574, April 11 (1995).

[9] G. Sh. Boltachev, N. B. Volkov and E. A. Chingina, Nanopowders in dynamic magnetic pulse compaction processes, *Nanotechnologies in Russia*, 9 (11) (2014) 650-659.

[10] V. P. Meshalkin and A. V. Belyakov, Methods used for the compaction and molding of ceramic matrix composites reinforced with carbon nanotubes, *Processes*, 8 (8) (2020).

[11] A. G. Mamalis, A. Szalay, N. Göbl, I. Vajda and B. Raveau, Near net-shape manufacturing of metal sheathed superconductors by high energy rate forming techniques, *Materials Science and Engineering: B*, 53 (1) (1998) 119-124.

[12] B. A. Kabert, High strain rate consolidation and forming of armstrong and HDH titanium powder and sheet material, *Master's Thesis*, The Ohio State University (2011).

[13] G. S. Boltachev, E. A. Chingina, A. V. Spirin and N. B.Volkov,

Densification rate influence on nanopowder compatibility, *Materials Physics and Mechanics*, 42 (2) (2019) 165-177.

[14] N. Thirupathi, R. Kumar and S. D. Kore, Experimental and numerical investigations on electromagnetic powder compaction of Aluminum 6061 alloy powder, *Powder Technology*, 406 (2022) 117579.

[15] F. Li, H. Li, X. Ge, J. Zhao, H. Wu, J. Lin and G. Huang, Numerical simulation of magnetic pulse radial compaction of W-Cu20 powder with a field shaper, *The International Journal of Advanced Manufacturing Technology*, 114 (1) (2021) 219-230.

Fenqiang Li is working as an Associate Professor in School of Materials Science and Engineering at Xiamen University of Technology in Xiamen, People's Republic of China. His research area includes electromagnetic forming, finite element analysis, and optimal design. He is also involved in numerous innovative studies. He completed his doctoral degree at Huazhong University of Science and Technology, People's Republic of China.